Quantum real wave-packet dynamics of the $N(^4S)+NO(\tilde{X}\,^2\Pi)\rightarrow N_2(\tilde{X}\,^1\Sigma_g^+)+O(^3P)$ reaction on the ground and first excited triplet potential energy surfaces: Rate constants, cross sections, and product distributions

Pablo Gamallo, R. Sayós, and Miguel González[a)]
Departament de Química Física i Centre de Recerca en Química Teòrica, Universitat de Barcelona i Parc Científic de Barcelona, C/Martí i Franquès 1, 08028 Barcelona, Spain

Carlo Petrongolo[b)] and Paolo Defazio
Dipartimento di Chimica, Universita' di Siena, Via Aldo Moro 2, 53100 Siena, Italy

(Received 2 November 2005; accepted 20 February 2006; published online 2 May 2006)

The reaction $N+NO\rightarrow N_2+O$ was studied by means of the time-dependent real wave-packet (WP) method and the *J*-shifting approximation. We consider the ground $1\,^3A''$ and first excited $1\,^3A'$ triplet states, which correlate with both reactants and products, using analytical potential energy surfaces (PESs) recently developed in our group. This work extends our previous quantum dynamics study, and probabilities, cross sections, and rate constants were calculated and interpreted on the basis of the different shapes of the PESs (barrierless $1\,^3A''$ and with barrier $1\,^3A'$ surfaces, respectively). The WP rate constant (k_1) shows a weak dependence on $T(200-2500\ \mathrm{K})$, as the dominant contribution to reactivity is provided by the barrierless ground PES. There is a good agreement of WP k_1 with the measurements and variational transition state theory (VTST) data, and also between the WP and VTST $k_1(1\,^3A'')$ results. Nevertheless, there is a large discrepancy between the WP and VTST $k_1(1\,^3A')$ results. Product state distributions were also calculated for the much more reactive $1\,^3A''$ PES. There is an excellent agreement with the experimental average fraction of vibrational energy in $N_2(25\pm3\%)$, the only measured dynamics property of this reaction. © *2006 American Institute of Physics*. [DOI: 10.1063/1.2186643]

I. INTRODUCTION

The gas phase bimolecular reaction of atomic nitrogen with nitric oxide,

$$N(^4S)+NO(\tilde{X}\,^2\Pi)\rightarrow N_2(\tilde{X}\,^1\Sigma_g^+)+O(^3P), \tag{1}$$

$[\Delta_r H^0_{0\ \mathrm{K}}=-75.01\ \mathrm{kcal\ mol^{-1}}$ (Ref. 1)] and its reverse reaction are chemical systems of a large atmospheric interest.[2] Reaction (1) has been the object of a significant number of kinetic experimental studies, but the experimental information available on the dynamics of this reaction is very scarce (N_2 product average vibrational energy fraction). From the theoretical point of view, considerable attention has been devoted to this reaction [*ab initio* calculations of the stationary points of the two lowest potential energy surfaces (PESs), analytical representations of the PESs, quasiclassical trajectory (QCT) calculations, and approximate quantum dynamics calculations].[2]

In recent contributions of our own, new analytical representations for the ground $1\,^3A''$ and first excited $1\,^3A'$ PESs were developed,[3] based on high level *ab initio* calculations, and variational transition state theory (VTST) rate constants[3] were calculated for reaction (1), its reverse and the O-atom exchange reaction,

$$N(^4S)+N'O(\tilde{X}\,^2\Pi)\rightarrow NO(\tilde{X}\,^2\Pi)+N'(^4S). \tag{2}$$

The comparison of the VTST rate constants with the experimental data (T:200–5000 K) showed an excellent agreement, and suggested the adequacy of both analytical PESs for kinetics and dynamics studies on this system.

Moreover, time-dependent real wave-packet (WP) quantum dynamics rate constants, cross sections, and microscopic reaction mechanism were determined on the $1\,^3A''$ analytical PES.[4] This WP calculation was done using the *J*-shifting approximation in the context of a capture model, as the ground surface is barrierless along the minimum energy path (MEP) leading from reactants to products. This surface, however, shows a high barrier [40.02 kcal mol^{-1}, including the zero point energy (ZPE)][3] for reaction (2). The analytical $1\,^3A'$ excited PES presents an energy barrier along the MEP of reactions (1) and (2) (8.74 and 27.45 kcal mol^{-1}, including the ZPE, respectively).[3] Thus, the $1\,^3A'$ barrier for the oxygen atom exchange process is smaller than in the case of the $1\,^3A''$ surface.

This contribution extends our previous quantum dynamics time-dependent real WP study on reaction (1).[4] In fact, here we consider the first excited PES, taking into account a large number of vibrorotational (v,j) levels of NO to accurately describe the kinetics and dynamics of this reaction. We also include a large number of additional calculations on the ground PES, considering much more NO vibrorotational levels than in Ref. 4, to better describe the reactivity of the

[a)]Electronic mail: miguel.gonzalez@ub.edu
[b)]Electronic mail: petrongolo@unisi.it

TABLE I. Parameters of the WP calculations. Values in a.u., unless otherwise specified.

Translational energy center of the initial WP	0.4 eV
R center and width of the initial WP	10 and 0.1
R' range and no. of grid points	0–14.5 and 329
r' range and no. of grid points	1.5–16.5 and 197
No. of Legendre polynomials and of γ' points	50 (including potential symmetry)
Potential and centrifugal cut off	0.44
R' and r' absorption start at	11.5 and 13.5
R' and r' absorption strength	0.01
Asymptotic analysis at R'	8.5

system. In addition to rate constants and cross sections, product state distributions have been calculated in the case of the dominant (much more reactive) $1\,^3A''$ ground PES.

The paper is organized as follows: The computational method is described in Sec. II; the reaction probabilities, cross sections, and rate constants are given in Sec. III; and Secs. IV and V contain the product distributions and the summary and conclusions, respectively.

II. METHOD

We use the time-dependent real WP method of Gray and Balint-Kurti (GBK),[5] which propagates a real WP under an arccos mapping of a shifted and scaled system Hamiltonian, via a Chebyshev time recursion. This approach is related to other WP techniques, as it can be seen, e.g., in Ref. 4. Here, the initial WP is defined in reactant Jacobi coordinates (R, r, and γ) and transformed into the product ones (R', r', and γ') for the subsequent time propagation and asymptotic analysis. As we did in our previous paper,[4] the $^{14}N_2$ permutation and nuclear-spin symmetries have also been taken into account. Thus, the $^{14}N_2(\tilde{X}\,^1\Sigma_g^+, v', j')$ vibrorotational states with j' =even or odd have nuclear statistical weights equal to 2/3 or 1/3, respectively.[6] The resulting reaction probabilities, resolved on the vibrorotational NO reactant state (v,j), at a total angular momentum quantum number J and collision energy $E_{\rm col}$, are given by

$$P^J_{vj}(E_{\rm col}) = \sum_{v'} \left\{ \frac{2}{3} \left[\sum_{j'={\rm even}} {}^{\rm even}P^J_{v'j',vj}(E_{\rm col}) \right] + \frac{1}{3} \left[\sum_{j'={\rm odd}} {}^{\rm odd}P^J_{v'j',vj}(E_{\rm col}) \right] \right\}, \quad (3)$$

where even and odd refer to the even and odd j' rotational quantum numbers of $^{14}N_2$ and $P^J_{v'j',vj}(E_{\rm col})$ are state-to-state reaction probabilities. By means of the GBK method,[5] accurate reaction probabilities are calculated for $J=0$ at $v=0-3$, $j=1-12$ in the collision energy interval of $0 \leqslant E_{\rm col} \leqslant 1.0$ eV, for both the ground and first excited PESs, with the parameters of Table I, whereas reaction probabilities for $J>0$ are estimated via the J-shifting approximation. The $1\,^3A''$ and $1\,^3A'$ surfaces (equipotential contour plots) are shown in Fig. 1.

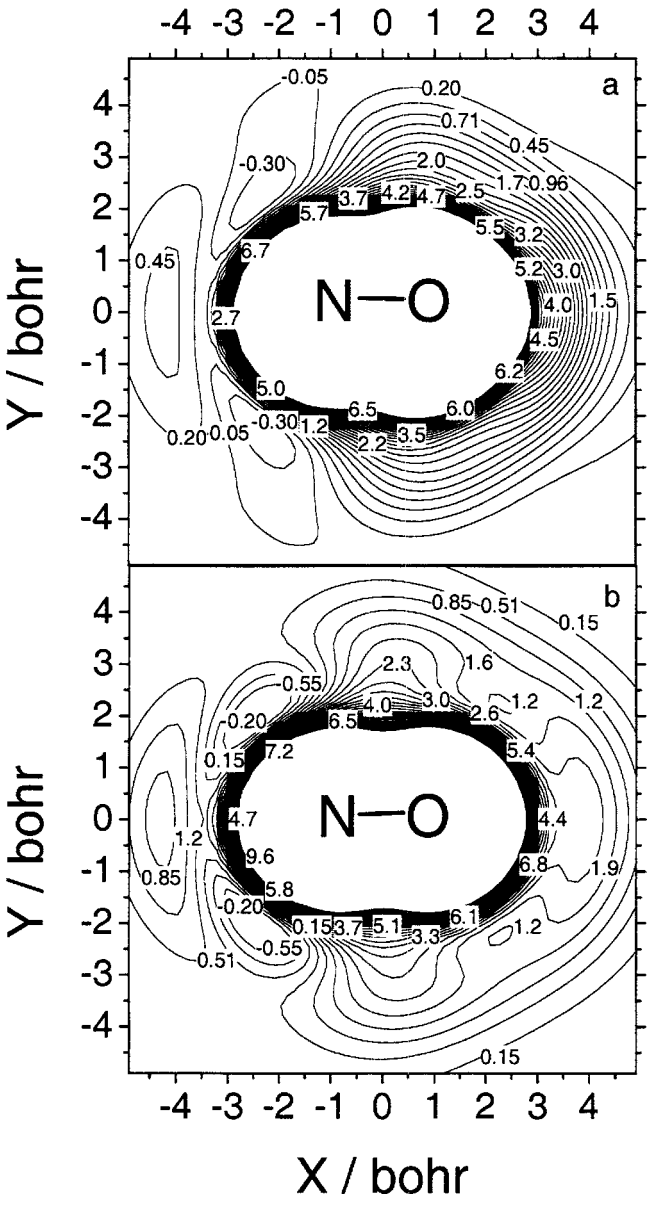

FIG. 1. Equipotential contour plots of the ground $1\,^3A''$ (a) and first excited $1\,^3A'$ (b) PESs for $r(\mathrm{NO})=2.17a_0$, as a function of the (x,y) coordinates of the N attacking atom. Energy is given in eV with respect to $\mathrm{N+NO}(r_{\rm eq})$.

As reaction (1) involves three heavy nuclei, both the exact and centrifugal-sudden[7] calculations for $J>0$ are very CPU-time demanding, and the J-shifting approximation is expected to be good enough to obtain reliable results.[4,8–10] This approximation estimates the reaction probabilities for $J>0$ according to

$$P^J_{vjK}(E_{\rm col}) \approx P^0_{vj0}(E_{\rm col} - E^{J\neq}_{jK}), \quad (4)$$

where the energy shift $E^{J\neq}_{jK}$ is evaluated in two different ways, depending on the nature (with barrier or barrierless surface) of the PES under consideration.

For the ground $1\,^3A''$ PES, as we explained in our previous paper,[4] the $E^{J\neq}_{jK}$ term is better called E^J_{jK}, due to the absence of transition state on this surface. Because of this and as in Ref. 4, we apply a capture model (CM),[10,11] assum-

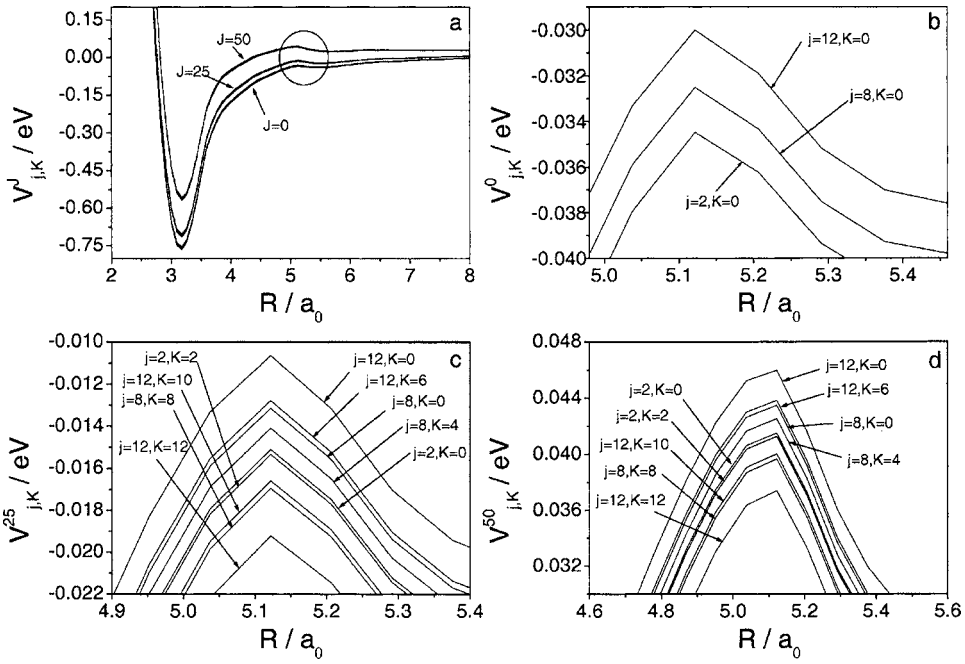

FIG. 2. Effective potentials $V^J_{jK}(R)$ of the $1\,^3A''$ PES for selected values of the J, j, and K quantum numbers [the encircled results in subfigure (a) are given in a more detailed way in subfigures (b)–(d)]. Dependence of $V^J_{jK}(R)$ on the following quantum numbers: (a) J (for $j=2$, 8, and 12, $K=0$, 4, 6, 10, and 12), (b) j (for $J=0$, $K=0$), (c) j and K (for $J=25$), and (d) j and K (for $J=50$). In the last two cases the following j and K values are considered: $j=2$, $K=0$ and 2, $j=8$, $K=0$, 4, and 8, and $j=12$, $K=0$, 6, 10, and 12.

ing that the early dynamics, before product formation, is dominated by effective potentials which have the following form:

$$V^J_{jK}(R) = \min_{r,\gamma} V(R,r,\gamma) + [J(J+1) + j(j+1) - 2K^2]/2\mu_R R^2, \quad r \leqslant 2.31a_0, \tag{5}$$

where $V(R,r,\gamma)$ is the ground state PES, K is the projection of $\boldsymbol{J}$ along $\boldsymbol{R}$, μ_R is the reduced mass associated with R, and the upper limit on r avoids the opening of the N_2+O product channel. The second term in the rhs member of Eq. (5) is the centrifugal potential. These effective potentials present centrifugal barriers that depend on three quantum numbers (J, j, and K). Therefore, the energy shifts E^J_{jK} are equal to

$$E^J_{jK} = \max_R V^J_{jK}(R) - \max_R V^0_{j0}(R). \tag{6}$$

In Eq. (5) we minimize the energy of the PES with respect to r and γ. For N+NO this is a better choice than Eq. (13) of Ref. 11, because the corresponding effective potentials present only shoulders as functions of J and K. Figure 2 shows several $V^J_{jK}(R)$ effective potentials for different sets of J, j, and K values. The effective potential $V^J_{jK}(R)$ increases with J and j, while decreases as K increases, as expected according to Eq. (5).

For the excited $1\,^3A'$ PES, the $E^{J\neq}_{jK}$ term is calculated in a much more direct way (standard case of a PES with an energy barrier), from the geometry of the transition state (nearly prolate symmetric top) of this surface, using the corresponding rotational constants ($\bar{B}^{\neq}=0.303$ cm^{-1} and $A^{\neq}-\bar{B}^{\neq}=2.626$ cm^{-1}),

$$E^{J\neq}_{jK} = \bar{B}^{\neq} J(J+1) + (A^{\neq} - \bar{B}^{\neq})K^2, \tag{7}$$

where $\bar{B}^{\neq}$ is the average of $B^{\neq}$ and $C^{\neq}$.

Initial-state-resolved cross sections $\sigma_{\nu j}(E_{\rm col})$ are obtained via the usual partial wave sum,[7] and rate constants $k_{\nu j}(T)$ and $k(T)$ are calculated as Boltzmann averages[12] in the 200–2500 K temperature range. The thermal rate constants k_1 for the $1\,^3A''$ and $1\,^3A'$ PESs are determined by estimating the $k_{\nu j}$ values for $j \geqslant 13$ via extrapolations. In fact, they were calculated assuming that the state-specific rate constants for NO rotational levels higher than 12 are equal to the rate constant for $j=12$ [$k_{\nu j}(j>12)=k_{\nu,12}$], as we have done in previous studies with good results.[4,9] This procedure is good enough for these PESs, because $k_{\nu j}$ does not vary much when changing the rotational level of NO.

The population of the electronic states involved, as a function of the temperature, has also been taken into account,[3,4] including both spin-orbit (SO) states of NO, $^2\Pi_{1/2}$ and $^2\Pi_{3/2}$, with their energy difference ($\Delta=119.82$ cm^{-1}),[13] through the following expression:

$$p^{\rm el}(T) = \frac{3}{4[2+2\exp(-\Delta/k_B T)]}, \tag{8}$$

where 3 and 4 are the degeneracies of the electronic states of the NNO system (identical in the $1\,^3A''$ and $1\,^3A'$ PESs) and N(^4S) atom, respectively, and the second term of the denominator is the NO electronic partition function. $p^{\rm el}(T)$ is the electronic factor that multiplies the rate constant values directly derived from the wave-packet calculations on each PES, and decreases with T from 0.264 to 0.194 in the 200–2500 K T interval.

The total rate constant k_1 for N_2+O generation through reaction (1) is then calculated by the sum of the $k_1(1\,^3A'')$ and $k_1(1\,^3A')$ rate constants, both already including the $p^{\rm el}(T)$ multiplicative term.

III. REACTION PROBABILITIES, CROSS SECTIONS, AND RATE CONSTANTS

Figure 3 shows eight examples of reaction probabilities, at the total angular momentum quantum number $J=0$, corresponding to the NO vibrorotational levels $\nu=0$–3, $j=1$ and 8, for both PESs.

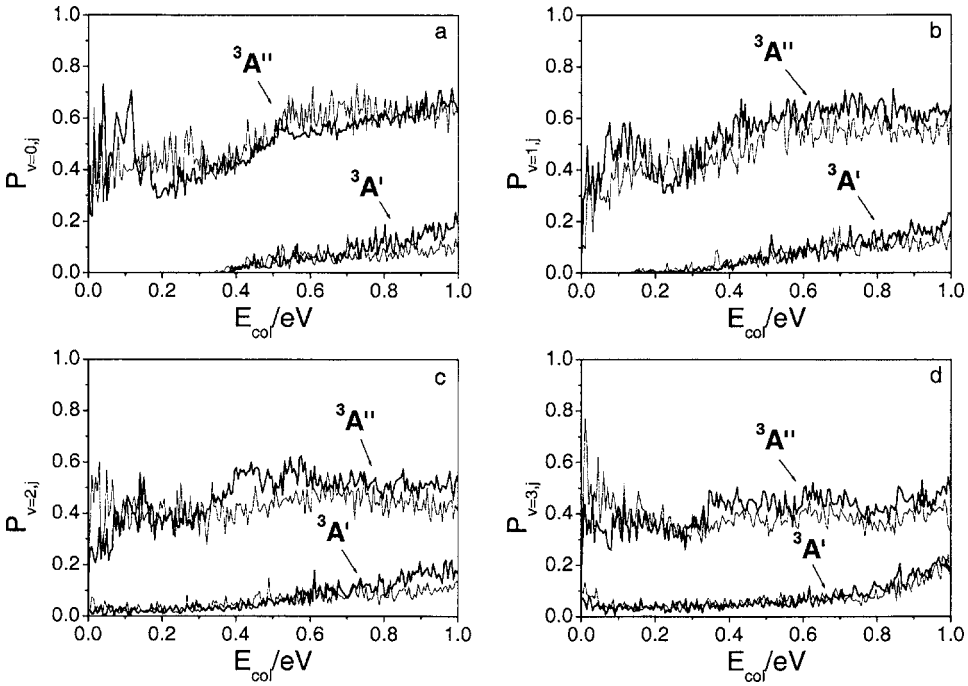

FIG. 3. Reaction probabilities for N $+$NO(ν=0–3,j)$\rightarrow$N$_2$$+$O as a function of E_{col}: j=1 (full line) and j=8 (dotted line), on the ground 1 $^3A''$ (upper curves) and excited 1 $^3A'$ (lower curves) PESs.

The ground 1 $^3A''$ PES has no reaction energy barrier along the MEP, and thus the reaction probabilities do not present energy threshold. By the contrary, the excited 1 $^3A'$ PES has an energy barrier along the MEP, and therefore a threshold energy appears for the levels ν=0 and 1, and j =1 and 8 (at E_{col} values of ~0.35 and 0.15 eV, respectively). However, for NO vibrational levels above ν=1, the internal energy of reactants becomes greater than the energy barrier and, consequently, no threshold energy is observed. Moreover, the significant barrier of the 1 $^3A'$ surface leads to reaction probabilities which, in general, are much smaller than those for the barrierless 1 $^3A''$ surface. The much larger reactivity exhibited by the ground potential energy surface will also be reflected both in the reaction cross sections and rate constants.

The NO rotational excitation tends to enhance the high-ν reaction probabilities, mainly at low collision energy, whereas at higher energies the opposite effect is observed for both PESs. The NO vibrational excitation has a little effect on the reactivity for the 1 $^3A''$ PES, in opposition to the 1 $^3A'$ PES, where the threshold energy plays an important role in dynamics when vibrational energy is increased. To help to understand these results, it is useful to analyze the effective interaction-centrifugal potentials. This analysis was already developed in our previous paper[4] and will not be considered further here.

Figures 4 and 5 present the reaction cross sections for the ν=0–3, j=1, 4, 8, and 12 NO vibrorotational levels on the 1 $^3A''$ and 1 $^3A'$ surfaces, respectively. The cross section of the ground PES decreases as collision energy increases

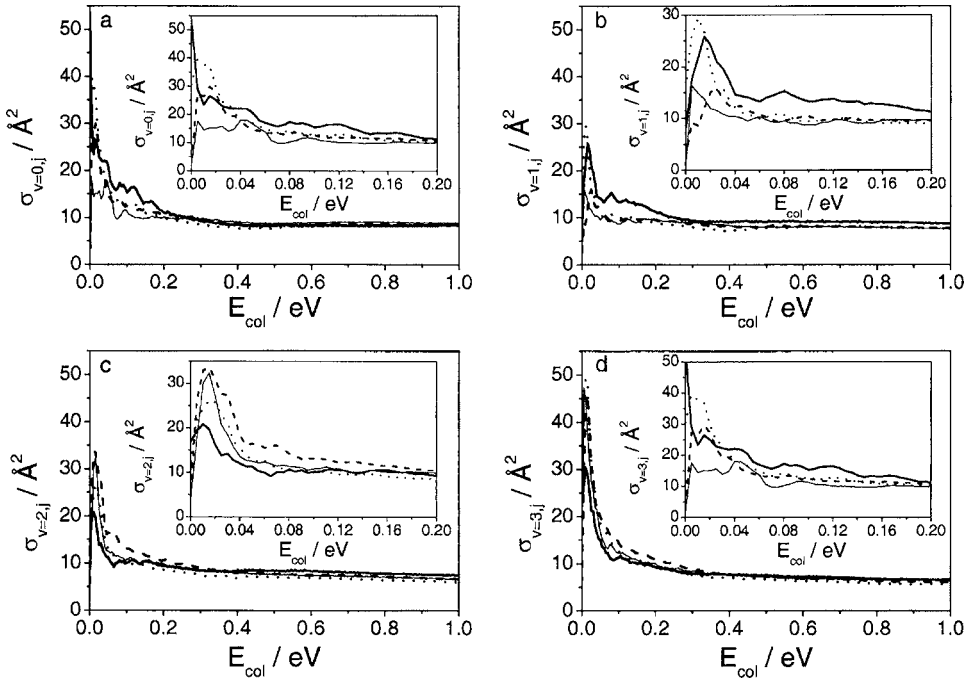

FIG. 4. Reaction cross sections for N $+$NO(ν=0–3,j)$\rightarrow$N$_2$$+$O as a function of E_{col}: j=1 (full line), j=4 (dotted line), j=8 (dashed line), and j =12 (thin full line), on the ground 1 $^3A''$ PES.

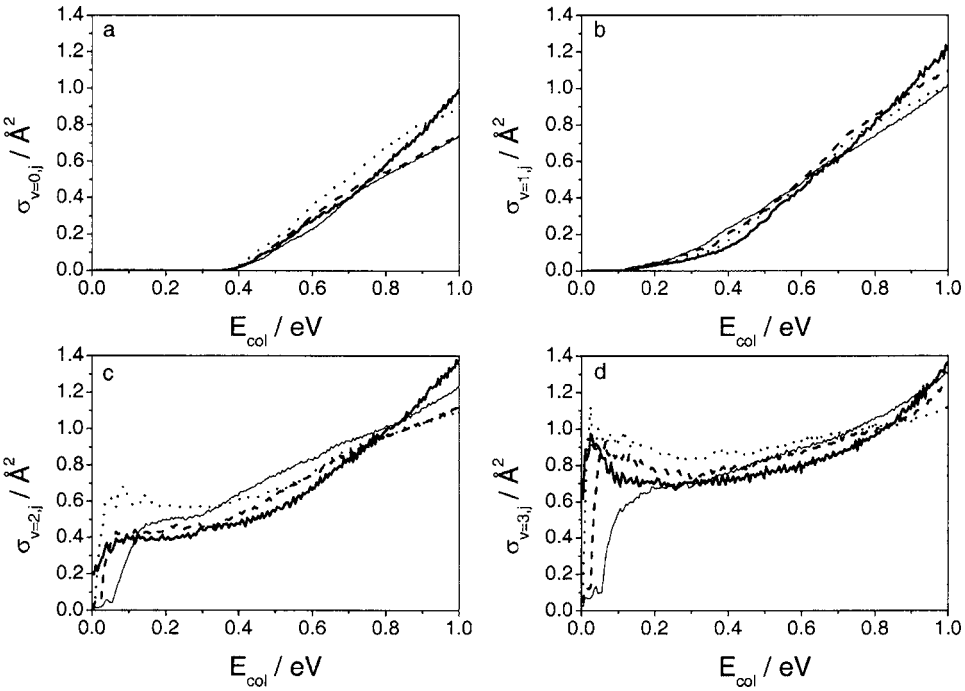

FIG. 5. Reaction cross sections for N $+$NO(v=0–3,j)$\rightarrow$N$_2$$+$O as a function of E_{col}: j=1 (full line), j=4 (dotted line), j=8 (dashed line), and j=12 (thin full line), on the excited 1 $^3A'$ PES.

from $\sim$0.015 to $\sim$0.20–0.40 eV, depending on the initial NO rotational level (Fig. 4). This is consistent[12] with a barrierless PES and with a long-range potential $V(R)\approx -C_s/R^s$ which dominates the dynamics at low E_{col}. For the excited PES, an energy threshold appears due to its energy barrier, but it disappears when $v\geqslant 2$ (Fig. 5), as the internal energy content of reactants is above the energy barrier. Some of the oscillations found in the reaction probabilities at low collision energies appear to be also evident in the reaction cross sections, mainly for the ground PES (E_{col} below 0.2 eV), but perhaps this result arises from the approximation (J-shifting) employed in the quantum dynamics calculations.

The WP initial-state-resolved cross sections for the 1 $^3A''$ PES are rather similar to the values reported in Ref. 14. However, this agreement is quite fortuitous, because the reaction cross sections of Ref. 14 were obtained using a semiempirical PES, employing the QCT method, and a Boltzmann distribution at 500 K of the NO vibrorotational states.

The reaction cross sections of the 1 $^3A'$ PES for v=0 and v=1 increase with collision energy in a roughly linear way, and in general the results are similar for different j values. For higher NO vibrational levels, an analogous effect is observed at intermediate-high collision energies, but at low collision energies this is not the case, and the more reactive rotational level is j=4.

Figures 6(a) and 6(b) show the initial-state-resolved rate constants $k_{vj}(T)$ at 300 and 2000 K, as a function of the NO vibrorotational level (v=0–3, j=1–12), for the 1 $^3A''$ and 1 $^3A'$ PESs, respectively. Increasing the NO excitation or the temperature, the 1 $^3A''$ reactivity varies at most by half a degree of magnitude, whereas the 1 $^3A'$ k_{vj} increase in a very significant way (up to five orders of magnitude) with v or T. The shape of the 1 $^3A''$ $k_{0j}(300)$ and $k_{1j}(300)$ rate constants are rather different from those of other rate constants ($k_{0j}>k_{1j}$ and both oscillate somewhat with j, mainly at low j values). For other initial conditions, or at 2000 K, these variations with j are, however, quenched. The 1 $^3A'$ k_{vj} rate constants are nearly independent on the NO rotational excitation. These results are consistent with the shape of both PESs: barrierless 1 $^3A''$ PES and important early barrier (i.e., transition state more similar to reactants than to products) in the case of the 1 $^3A'$ PES. In particular, according to Polanyi's rules,[12] collision (translational) energy is particularly efficient to reach products in the case of an early barrier potential energy surface.

Table II compares the WP, ICVT,[3] and ICVT/μOMT-SO[3] thermal rate constants $k_1(T)$. Although it was not mentioned in Ref. 3, it is important to indicate that in reaction (1), for both the ground and excited surfaces, the conventional TST and VTST [at the improved canonical VTST (ICVT) level] methods lead to very similar results. This means that for reaction (1) recrossing is not relevant, as expected on the basis of the reaction kinematics (heavy-heavy-heavy mass combination). In addition, tunneling plays in general a minor contribution to the rate constant of the reaction, as the imaginary frequency of the 1 $^3A'$ transition state is quite small. On the other hand, different approaches (SCT and μOMT methods) to deal with the tunneling contribution to reactivity in the VTST context lead to the same results, and the simple Wigner tunneling correction of the TST results leads to values which are very close to the VTST $+$tunneling correction ones.

Table III shows the WP, ICVT, and ICVT/μOMT-SO total rate constants [$k_1=k_1(1\ ^3A'')+k_1(1\ ^3A')$] and the recommended[15,16] and laboratory[17–19] measured values, within the 200–2500 K temperature interval. WP rate constants (in cm^3 s^{-1}) were also bestfitted to the following equation:

$$k_1(T)=AT^n\exp(B/T), \tag{9}$$

where $A=(4.35\pm0.04)\times10^{-12}$ cm^3 s^{-1} K$^{-0.28}$, $n=0.28\pm0.01$, and $B=130.68\pm6.85$ K.

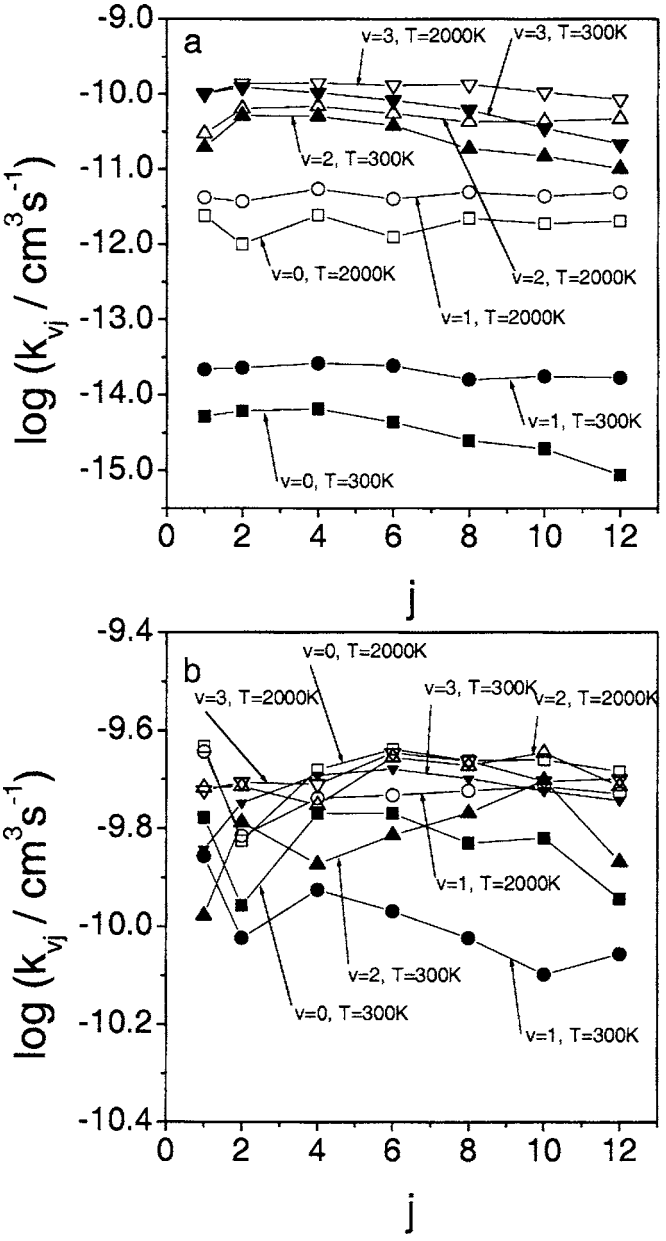

FIG. 6. Initial-state-specific $N+NO(\nu,j)\rightarrow N_2+O$ reaction rate constants on the ground $1\,^3A''$ (a) and excited $1\,^3A'$ (b) PESs.

Table III shows that the total reaction rate constant is practically independent of temperature, but two types of behavior appear in the 200–2500 K T interval. The first behavior is observed from 200 to 500 K, where the reaction rate decreases as T increases. This effect is directly related with the fact that at low temperatures, reaction (1) mainly evolves on the ground PES (negative values of the activation energy are related with barrierless PESs). Above 500 K, as T increases the rate constant increases. This behavior is noted in the analysis of the ground PES behavior, but it is enhanced by the excited PES, as its contribution to reactivity progressively increases with temperature, as expected for a PES with an energy barrier. Nevertheless, in the T range explored (200–2500 K) the ground PES is much more reactive than the excited one.

The WP and ICVT/μOMT-SO[3] rate constants are in quite good agreement within the temperature range considered, although they are somewhat different. Indeed, for $T \leqslant 300$ K the statistical rate constant seems to be too large, and the opposite occurs above 600 K where there is a slope change. The contribution of the excited $1\,^3A'$ PES to the thermal rate constant is negligible up to 2000 K, where it becomes maximal and equal to 4%. This value is smaller than the 7% of contribution derived from the ICVT/μOMT-SO[3] statistical method.

The WP rate constant values are in excellent agreement with laboratory[17–19] and recommended[15,16] values, and, in particular, with the rate constant results of Ref. 19. Moreover, the WP rate constant data are different from those inferred in models of planetary atmospheres.[20,21] This suggests that these models are incorrect and/or the planetary populations of the reactants do not correspond to the thermal conditions studied in the laboratories.[14]

IV. PRODUCT DISTRIBUTIONS

The state-to-state dynamics of $N+NO(\nu,j)\rightarrow N_2(\nu',j')+O$ is important in nonequilibrium reaction conditions among the several degrees of freedom (translational, vibrational, and rotational) involved, as occurs in high-speed gases around aircraft jets and reentering spacecrafts.[22] In this section we thus present state and energy distributions of the N_2+O products, both initial-state-resolved and thermal, on the ground $1\,^3A''$ PES, which is much more reactive than the excited $1\,^3A'$ PES. For reader's convenience, we plot in Fig. 7 an energy diagram with respect to the N_2+O PES minimum. For the N+NO reactants, we show the PES minimum at 3.29 eV and the NO ground vibrorotational level ($\varepsilon_{01}=3.41$ eV). For the N_2+O products, we show 1163 vibrorotational levels $\varepsilon_{\nu'j'}$, with $j' \leqslant 99$ and up to 4.3 eV. Many vibrorotational channels $N_2(\nu',j')+O$ are open in this energy range, owing to the large nuclear masses and exoergicity of the reaction.

Following our previous paper[23] on $LiH(\nu,j)+H\rightarrow Li+H_2(\nu',j')$, product distributions are based on state-to-state cross sections $\sigma_{\nu'j',\nu j}(E_{\mathrm{col}})$ and state-to-state rate constants $k_{\nu'j',\nu j}(T)$. Nevertheless, our cross section definition does not take into account the T-dependent population $p^{\mathrm{el}}(T)$ of the NNO electronic state $1\,^3A''$, given in Eq. (8). Because the experimental observables are electronic-weighted cross sections $p^{\mathrm{el}}(T)\sigma_{\nu'j',\nu j}(E_{\mathrm{col}})$, we here simulate a room-temperature experiment, and report $p^{\mathrm{el}}(300)\sigma_{\nu'j',\nu j}(E_{\mathrm{col}})$, $p^{\mathrm{el}}(300)\sigma_{\nu',\nu j}(E_{\mathrm{col}})$, and $p^{\mathrm{el}}(300)\sigma_{\nu j}(E_{\mathrm{col}})$, with $p^{\mathrm{el}}(300)=0.2399$. The vibrational-resolved and initial-state-resolved quantities are derived summing over j' and (ν',j'), respectively. Of course, the rate constant definition already includes the electronic population.

As in Ref. 23, we also report energy and thermal distributions of products. The initial-state-resolved energy distribution is obtained from the vibrational, rotational, and translational energies, $E'^{\mathrm{vib}}_{\nu j}(E_{\mathrm{col}})$, $E'^{\mathrm{rot}}_{\nu j}(E_{\mathrm{col}})$, and $E'^{\mathrm{tr}}_{\nu j}(E_{\mathrm{col}})$, respectively. We calculate thermal state distributions $D_{\nu'j'}(T)$ and $D_{\nu'}(T)$ and thermal energy distributions $E'^{\mathrm{vib}}(T)$, $E'^{\mathrm{rot}}(T)$, and $E'^{\mathrm{tr}}(T)$, by Boltzmann averaging the $k_{\nu'j',\nu j}(T)$ rate constants over the initial states.

TABLE II. Theoretical WP and VTST rate constants (in $cm^{-3}\,s^{-1}$) for the $1\,^3A''$ and $1\,^3A'$ PESs.

T/K	WP $k_1(1\,^3A'')$ $(\times 10^{11})$	VTST[a] $k_1(1\,^3A'')$ $(\times 10^{11})$	WP $k_1(1\,^3A')$	VTST[b] $k_1(1\,^3A')$	VTST[c] $k_1(1\,^3A')$
200	3.66	6.51	5.90×10^{-18}	1.57×10^{-21}	2.20×10^{-21}
300	3.38	4.67	7.35×10^{-18}	2.31×10^{-18}	2.68×10^{-18}
400	3.27	3.78	3.49×10^{-17}	9.34×10^{-17}	1.01×10^{-16}
500	3.23	3.39	2.71×10^{-16}	8.93×10^{-16}	9.41×10^{-16}
600	3.23	3.19	1.26×10^{-15}	4.14×10^{-15}	4.29×10^{-15}
800	3.29	3.05	9.63×10^{-15}	2.98×10^{-14}	3.04×10^{-14}
1000	3.39	3.02	3.50×10^{-14}	1.02×10^{-13}	1.03×10^{-13}
1250	3.53	3.01	1.02×10^{-13}	2.85×10^{-13}	2.88×10^{-13}
1500	3.67	3.01	2.11×10^{-13}	5.85×10^{-13}	5.88×10^{-13}
1750	3.80	3.03	3.54×10^{-13}	9.99×10^{-13}	1.00×10^{-12}
2000	3.89	3.06	5.17×10^{-13}	1.52×10^{-12}	1.52×10^{-12}
2500	4.00	3.18	8.52×10^{-13}	2.82×10^{-12}	2.83×10^{-12}

[a]The ICVT-SO data were calculated but no reported in Ref. 3 and are identical to the ICVT/μOMT-SO results. For the $1\,^3A''$ PES VTST only no scaled data were calculated in Ref. 3, as this surface has no energy barrier along the MEP.
[b]ICVT-SO no scaled data for the $1\,^3A'$ PES, calculated but not reported in Ref. 3.
[c]ICVT/μOMT-SO no scaled data for the $1\,^3A'$ PES, calculated but not reported in Ref. 3.

A. Initial-state-resolved distributions

We present initial-state-resolved distributions from NO in the ground vibrorotational state (0,1). As Fig. 8 shows, the initial-state-resolved cross section $p^{el}(300)\sigma_{01}$ in general decreases versus collision energy, as expected for a barrierless PES. However, there are several oscillations which vanish as E_{col} increases. This appears to be a direct consequence of the shape of the reaction probability as a function of collision energy (see Fig. 3). Thus, it is interesting to see that quantum effects are also evident in the $p^{el}(300)\sigma_{01}$ observable.

Figure 9(a) reports the vibrorotational cross sections $p^{el}(300)\sigma_{2j',01}(E_{col})$ at $E_{col}=0.005$ and 1.0 eV vs j'. We clearly see a sawtoothed distribution due the Bose-Einstein statistics of the $^{14}N_2$ nuclear spins. Even j' states (*ortho*-N_2) are indeed about twice more populated that near-neighboring odd j' states (*para*-N_2), because the former are associated with singlet or quintet nuclear states, and the latter are associated with triplet nuclear states.[6] At $E_{col}=0.005$ eV, the largest cross section corresponds to $j'_{max}=36$, the rotational distribution is sharp, and the reaction is very state selective. For example, at $v'=2$ only 16 rotational states of $N_2(2,j')$ are appreciably populated $[p^{el}(300)\sigma_{2j',01}(E_{col})$ larger than 0.05 $Å^2]$, with $30\leqslant j'\leqslant 48$, among 100 states that are available. Increasing E_{col} up to 1.0 eV, the rotational distribution is similar, except for the larger available energy which is a little redistributed over more final states and $j'_{max}=34$. This implies that the reactant collision energy does not flow into the product rotational mode, as we shall also see later on.

The even-odd j' intensity alternation is present at all vibrational manifolds v', as we see, e.g., in Fig. 9(b), that shows the nascent product spectrum of $^{14}N_2(v',j')$, from N $+NO(v=0,j=1)$ at $E_{col}=0.005$ eV vs the vibrorotational lev-

TABLE III. Theoretical (WP and VTST) and experimental total rate constants ($k_1\times10^{11}$ in $cm^3\,s^{-1}$).

T/K	WP	VTST[a]	VTST[b]	Recommended[c]	Recommended[d]	Laboratory[e]	Laboratory[f]
200	3.66	6.51	6.51	3.9±1.6		3.5±1.1	
300	3.38	4.67	4.67	3.0±0.8		3.5±1.1	2.5±1.3
400	3.27	3.78	3.78	2.9±1.0		3.5±1.1	3.2±1.4
500	3.23	3.39	3.39			3.5±1.1	3.9±1.5
600	3.23	3.19	3.19			3.5±1.1	4.4±1.6
800	3.29	3.06	3.06			3.5±1.1	
1000	3.39	3.04	3.04			3.5±1.1	
1250	3.54	3.06	3.06			3.5±1.1	
1500	3.69	3.11	3.11		4.7±2.0	3.5±1.1	
1750	3.84	3.18	3.19		5.0±2.2	3.5±1.1	
2000	3.94	3.29	3.29		5.3±2.3	3.5±1.1	
2500	4.09	3.56	3.57		5.8±2.5	3.5±1.1	

[a]ICVT-SO no scaled data calculated but not reported in Ref. 3.
[b]ICVT/μOMT-SO no scaled data from Ref. 3.
[c]Reference 16.
[d]Reference 15.
[e]Reference 19. k_1 is constant in the full temperature range.
[f]Reference 18.

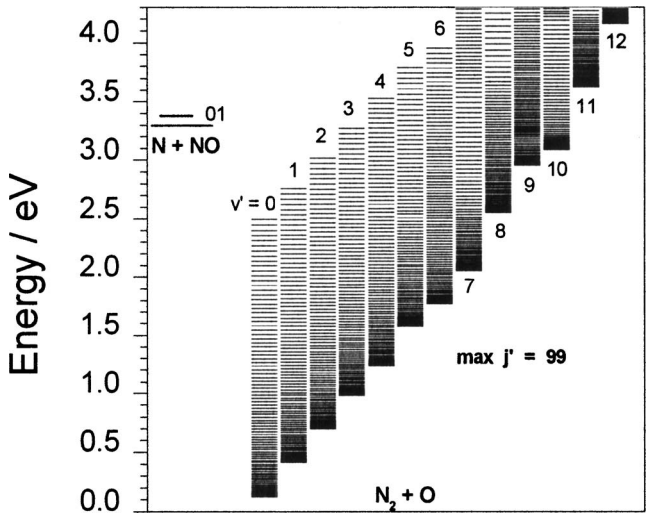

FIG. 7. NO ground vibrorotational energy level (ε_{01}) and N_2 vibrorotational energy levels ($\varepsilon_{\nu' j'}$) for $j' \leqslant 99$. Energies are given with respect to the N_2 +O PES minimum.

els ($\varepsilon_{\nu' j'}$). For each N_2 vibrational manifold, we also present the $j'_{\max}$ value of the largest cross section. At 0.005 eV, the collision populates preferentially 55 N_2 levels, which are placed between ~0.7 and 1.7 eV above the product PES minimum (see Fig. 7), with cross sections larger than 0.05 Å^2, whereas 895 $N_2(\nu', j')$ levels are open in this energy range. The largest cross section $\sigma_{\nu' j',01}$ is associated with the $N_2(2,36)$ state, which is placed at 1.04 eV, i.e., 0.90 eV above the $N_2(0,0)$ ground level. The N_2 vibrorotational spectrum presents seven clear vibrational bands up to $\nu'=6$. N_2 channels with $\nu' \geqslant 7$ are thus dynamically closed at low collision energy, although many of them are energetically open, as Fig. 7 shows. Each vibrational band consists of few rotational lines stronger than 0.005 Å^2, with $j'_{\max}$ between 36 and 42. These bands are thus little overlapping, save those with $\nu'=3$ and 4 that have rather long blue and red tails, respectively. Therefore, the N_2 nascent vibrational spectrum is rather wide, but the rotational spectrum is quite narrow. This is consistent with a large rotational selectivity, and is reflected on the product orbital angular momentum quantum number L'. Taking indeed into account the triangular condition $|J-L'| \leqslant j' \leqslant J+L'$ and the small J range associated with the low $E_{\rm col}$ value, this small j' range implies that L' is rather small. Hence, the N_2 rotational distribution at low collision energies is consistent with the relatively narrow minimum energy path of the $1\,^3A''$ PES, which forces a proper orientation of the N and NO reactants for the reaction to occur (stereospecific bent abstraction).[3]

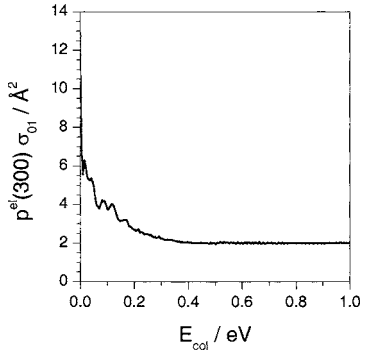

FIG. 8. N+NO($\nu=0, j=1$)$\rightarrow N_2$+O electronic-weighted cross section $p^{\rm el}(300)\sigma_{01}(E_{\rm col})$ on the $1\,^3A''$ PES vs $E_{\rm col}$.

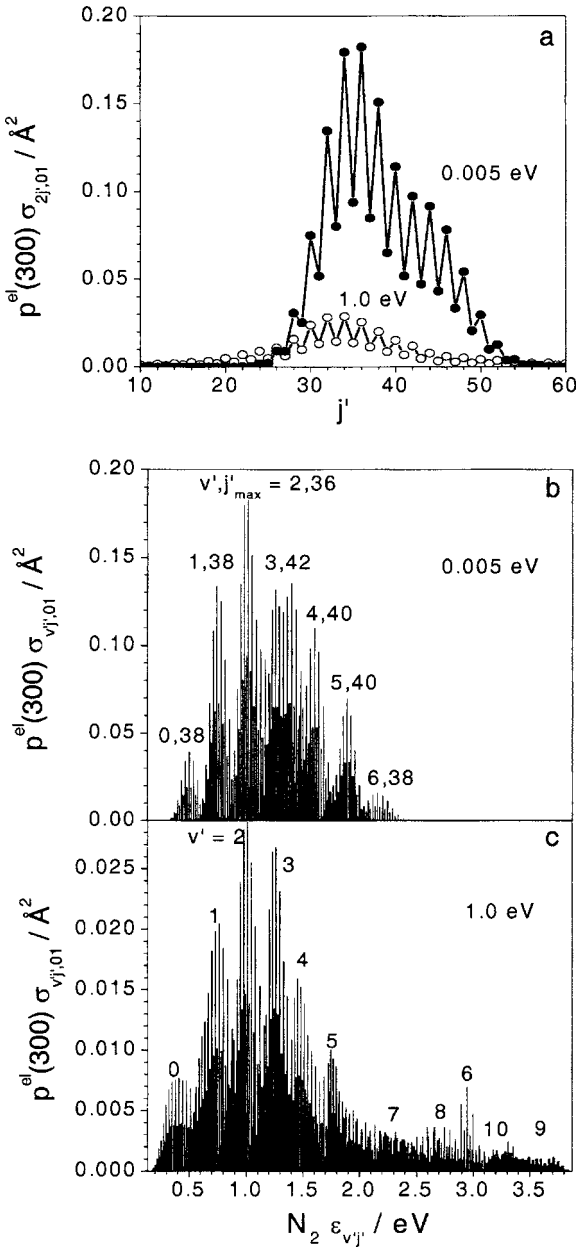

FIG. 9. N+NO($\nu=0, j=1$)$\rightarrow N_2(\nu', j')$+O electronic-weighted cross sections $p^{\rm el}(300)\sigma_{\nu' j',01}(E_{\rm col})$ on the $1\,^3A''$ PES. Panel (a) shows the results for $\nu'=2$ at two $E_{\rm col}$ values vs j'. Panels (b) and (c) show the results at $E_{\rm col}$ =0.005 and 1.0 eV, respectively, vs the vibrorotational energy levels of $N_2(\varepsilon_{\nu' j'})$.

We present the N_2 vibrorotational distribution for N +NO($\nu=0, j=1$) at $E_{\rm col}$=1.0 eV in Fig. 9(c), with a different cross section scale with respect to that of panel (b). When N_2 states are open at any collision energy, their state-to-state cross sections $\sigma_{\nu' j',01}$ decrease versus $E_{\rm col}$, as the initial-state-resolved σ_{01} does (Fig. 8). As collision energy increases, more N_2 vibrational channels are open, the rotational distribution is smoother, and presents long tails at low and high j'. The vibrational bands thus overlap progressively more, mainly for highly excited N_2 states, and reactive col-

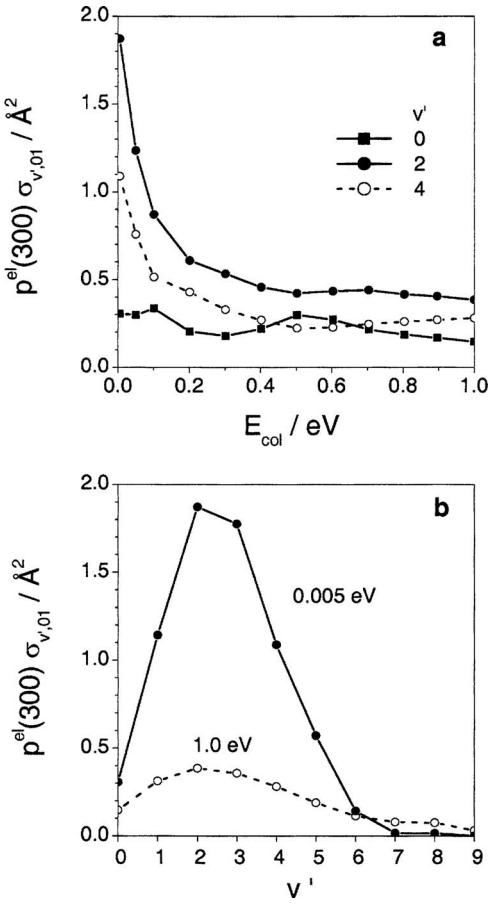

FIG. 10. N+NO($\nu=0,j=1$)$\rightarrow$N$_2$(ν')+O electronic-weighted cross sections $p^{el}(300)\sigma_{\nu',01}(E_{col})$ on the $1\,^3A''$ PES vs E_{col} (a), and vs ν' (b).

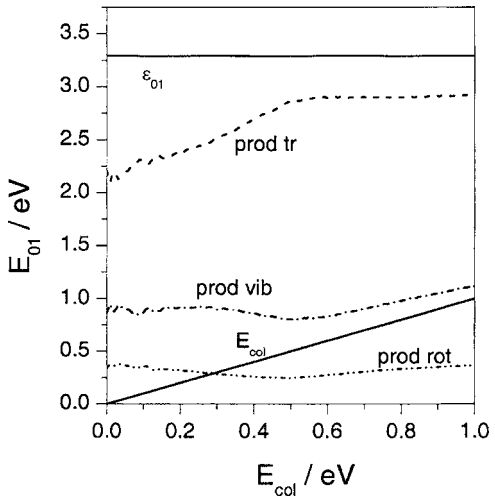

FIG. 11. N+NO($\nu=0,j=1$)$\rightarrow$N$_2$+O product energy distribution on the $1\,^3A''$ PES vs E_{col}.

lisions become less state selective, as expected. Comparing Figs. 9(b) and 9(c), wee see that the rotational peaks of the vibrational bands with $\nu' \leqslant 5$ are shifted to the red. This shift is maximum at $\nu'=5$ and equal to 0.20 eV (from $j'_{max}=40$ at $E_{col}=0.005$ eV to $j'_{max}=26$ at $E_{col}=1.0$ eV). Figure 9(c) also shows a different N$_2$ vibrorotational distribution at $\varepsilon_{\nu'j'}$ larger than $\sim$2 eV. We see indeed an inverted vibrational distribution, where the maximum intensity of the $\nu'=6$ band is at the blue of those at $\nu'=7$ and 8. With respect to Fig. 9(b), the maximum at $\nu'=6$ is thus blueshifted by 0.73 eV, with an increase of 30 quanta (from 38 to 68) in j'_{max}.

We plot in Fig. 10 the vibrational cross sections $p^{el}(300)\sigma_{\nu',01}$ vs E_{col} and ν', in panels (a) and (b), respectively. Figure 10(a) reports representative results for $\nu'=0$, 2, and 4, and shows that $\sigma_{2,01}$ is the largest cross section at any E_{col} value, this being more evident at the lower energies explored. Moreover, $\sigma_{0,01}$ slightly oscillates, and the $\sigma_{\nu',01}$ cross sections, with $\nu'>0$, decrease versus E_{col} like σ_{01}. When we plot $p^{el}(300)\sigma_{\nu',01}$ vs ν' [Fig. 10(b)] we obtain an inverted vibrational distribution, which is peaked at $\nu'=2$ and 3 at any collision energy, although it is of course smoother at larger E_{col} values. This agrees with what is expected from Polanyi's rule for an exoergic and barrierless reaction.[12] The average $\bar{\nu}'$ value increases from $\sim$2.5 at $E_{col}=0.005$ eV to $\sim$3.3 at $E_{col}=1.0$ eV.

Figure 11 presents the product energy distribution of the N+NO(0,1) reaction, as a function of collision energy. We plot E'^{tr}_{01}, E'^{vib}_{01}, and E'^{rot}_{01} vs E_{col}, together with the NO internal energy (ε_{01}) and E_{col}. When the collision energy is very small, we observe a predominant internal-to-translational energy redistribution, with product average energy fractions $f'^{tr}_{01}=65\%$, $f'^{vib}_{01}=25\%$, and $f'^{rot}_{01}=10\%$. Increasing the collision energy up to 1.0 eV, these energy fractions do not vary appreciably, but we find an energy flow from the reactant collision mode to the product recoil one up to $E_{col}\approx 0.5$ eV, and a collision-to-vibrational energy transfer at higher E_{col} values. The latter result is associated with $\Delta E'^{vib}_{01}=0.25$ eV, i.e., with an increase of about one vibrational quantum of N$_2$, in agreement with the $\sigma_{\nu',01}$ results we discussed above.

B. Thermal distributions

We consider temperatures up to 1000 K, and report product thermal distributions due to NO($0,j$) excited rotational states. Indeed, only the ground vibrational state of NO is appreciably populated in this T range.

The Boltzmann average over the NO($0,j$) initial states, and the Maxwell average over the collision energy, affect little the distribution we discussed in Sec. IV A. We thus present only the vibrational distribution $D_{\nu'}(T)$ in Fig. 12. Panel (a) of this figure shows that the distribution is inverted at any T, with $\nu'=2$ preferred up to $\sim$400 K, and $\nu'=3$ preferred at higher temperatures. All $D_{\nu'}$ vary monotonically with T, save D_3 that has a small maximum at 300 K. As temperature increases, we find an overall population redistribution from $\nu'=1$ and 2 to $\nu'=4-8$. Panel (b) summarizes the results at 100 and 1000 K, showing that $D_{\nu'}(100)$ is a bit sharper than the hotter distribution $D_{\nu'}(1000)$, as expected. These thermal results versus T are qualitatively similar to the initial-state-resolved ones of Fig. 10(b) versus E_{col}, although the former are vibrationally hotter as T increases. This reflects the role of the NO($0,j$) excited rotational states, and the integration over the collision energy values.

Finally, we briefly note that the fractions of product energies under thermal reaction conditions are nearly constant in the temperature range investigated, with $f'^{tr}=66\%$, $f'^{vib}=24\%$, and $f'^{rot}=10\%$. These values are close the initial-

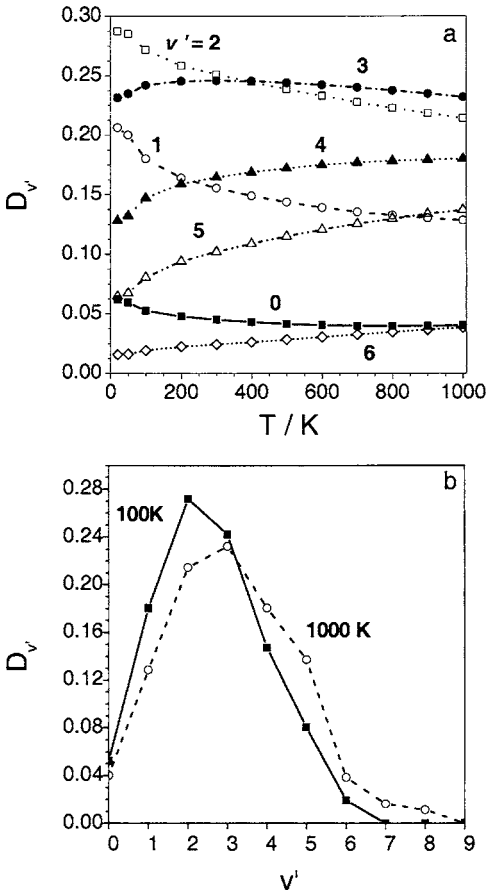

FIG. 12. Vibrational distributions $D_{v'}(T)$ of N_2 on the $1\,^3A''$ PES from thermal N+NO, represented in two different ways.

state-resolved ones, and the calculated vibrational energy fraction is in excellent agreement with the experimental value of $25\pm3\%$.[24]

V. SUMMARY AND CONCLUSIONS

The reaction $N(^4S)+NO(\tilde{X}\,^2\Pi)\rightarrow N_2(\tilde{X}\,^1\Sigma_g^+)+O(^3P)$ has been studied by means of the time-dependent real wave-packet quantum dynamics method and the *J*-shifting approximation, considering the two most relevant PESs (ground $1\,^3A''$ and first excited $1\,^3A'$ PESs) and employing recent *ab initio* based analytical representations developed in our group for both surfaces.

This contribution extends our previous WP study on reaction (1), taking into account the excited PES and a much larger number of vibrorotational levels of $NO(v=0-3, j=1-12)$ than in the previous work, for both surfaces. Reaction probabilities, cross sections, and rate constants for reaction (1) have been calculated. The dependences on collision energy and vibrorotational levels of NO have been interpreted taking into account the different shapes of the ground and excited PESs (barrierless and with barrier surfaces, respectively).

The WP rate constant of reaction (1), $k_1=k_1(1\,^3A'')+k_1(1\,^3A')$, which shows a weak dependence on temperature (T:200–2500 K), because the dominant contribution to the reactivity is provided by the ground PES, has been compared with previous VTST (ICVT level), VTST+tunneling (ICVT/μOMT level), and experimental results. There is a good agreement with the measurements, when the experimental uncertainties are accounted for, and also with the ICVT and ICVT/μOMT data, although this agreement progressively diminishes from 300 to 200 K. There is also a good accord in the case of the WP and ICVT/μOMT $k_1(1\,^3A'')$ results, because reactivity is clearly dominated by the ground PES in the T interval explored. However, there is a significant discrepancy between the WP and ICVT/μOMT $k_1(1\,^3A')$ results. Thus, within the 200–1000 K T range the WP $k_1(1\,^3A')$ values are much smaller than the ICVT/μOMT ones (with the exception of what happens at the lowest temperature explored), and in the 1250–2500 K interval the WP $k_1(1\,^3A')$/ICVT/μOMT $k_1(1\,^3A')$ ratio is almost constant and approximately equal to 0.34. After many checks we have been unable to understand the reasons of this discrepancy, which however little affects the k_1 values, as reactivity is dominated by the ground $1\,^3A''$ PES.

In addition to rate constants and cross sections, product state distributions have been calculated in the case of the much more reactive ground surface. The nascent $N_2(v',j')$ spectrum due to N+NO(0,1) is more intense at low E_{col}, as reactivity is larger, and it is formed by rather separated vibrational bands, with the v' distribution inverted. The rotational distribution is very selective, because only 6% of the open N_2 rotational channels is appreciably populated at $E_{col}=0.005$ eV. Moreover, in agreement with the $^{14}N_2$ nuclear-spin statistics, we find a j' intensity alternation, with even rotational levels about twice stronger than odd ones. Finally, the recoil and vibrational energies of products are equal to 65% and 25% of the total available energy of the collision, respectively. Unfortunately, there is no experimental dynamics information on this system to compare with, with the only exception of the average fraction of vibrational energy in N_2, where an excellent agreement has been found between the WP calculations (24%) and the measurements ($25\pm3\%$).

ACKNOWLEDGMENTS

This work was supported by the Spanish Ministry of Science and Technology (Projects BQU2002-04269-C02-02 and BQU2002-03351), Spanish Ministry of Education and Science (Project CTQ2005-09334-C02-01), MIUR, University of Siena, and IPCF-CNR of Pisa, Italy. The authors are also grateful to the collaborative project ("Integrated Action") Barcelona-Siena (Refs. HI2004-0094 and IT2169), to the "Generalitat de Catalunya" (Refs. 2001SGR 00041 and 2005SGR 00175), and to the "Centre de Supercomputació i Comunicacions de Catalunya" (C-CESCA/CEPBA). One of the authors (P.G.) thanks the University of Barcelona for a predoctoral research grant and another author (P.D.) thanks the help provided by the HPC-Europe program.

[1] M. W. Chase, Jr., C. A. Davies, J. R. Downey, Jr., D. J. Frurip, R. A. McDonald, and A. N. Syverud, J. Phys. Chem. Ref. Data Suppl. **14**, 1 (1985).
[2] P. Gamallo, M. González, and R. Sayós, J. Chem. Phys. **118**, 10602 (2003), and references therein.
[3] P. Gamallo, M. González, and R. Sayós, J. Chem. Phys. **119**, 2545 (2003).

[4] P. Gamallo, M. González, R. Sayós, and C. Petrongolo, J. Chem. Phys. **119**, 7156 (2003).
[5] S. K. Gray and G. G. Balint-Kurti, J. Chem. Phys. **108**, 950 (1998).
[6] G. Herzberg, *Molecular Spectra and Molecular Structure* (Krieger, Malabar, Florida, 1989), Vol. I, p. 134.
[7] R. T. Pack, J. Chem. Phys. **60**, 633 (1974).
[8] J. M. Bowman, Adv. Chem. Phys. **61**, 115 (1985); J. M. Bowman, J. Phys. Chem. **95**, 4960 (1991).
[9] P. Defazio, C. Petrongolo, C. Oliva, M. González, and R. Sayós, J. Chem. Phys. **117**, 3647 (2002).
[10] I. Miquel, M. González, R. Sayós, G. G. Balint-Kurti, S. K. Gray, and E. M. Goldfield, J. Chem. Phys. **118**, 3111 (2003).
[11] S. K. Gray, G. G. Balint-Kurti, G. C. Schatz, J. J. Lin, X. Liu, S. Harich, and X. Yang, J. Chem. Phys. **113**, 7330 (2000).
[12] R. D. Levine and R. B. Bernstein, *Molecular Reaction Dynamics and Chemical Reactivity* (Oxford University Press, New York, 1987).
[13] K. P. Huber and G. Herzberg, *Molecular Spectra and Molecular Structure* (Van Nostrand, New York, 1979), Vol. IV, p. 476.
[14] W. Duff and R. D. Sharma, Geophys. Res. Lett. **23**, 2777 (1996).
[15] D. L. Baulch, C. J. Cobos, R. A. Cox *et al.*, J. Phys. Chem. Ref. Data **23**, 847 (1994), and references therein.
[16] W. B. DeMore, S. P. Sander, C. J. Howard, A. R. Ravinshankara, D. M. Golden, C. E. Kolb, R. F. Hampson, M. J. Kurylo, and M. J. Molina, *Chemical Kinetics and Photochemical Data for Use in Stratospheric Modeling* (NASA-JPL, Pasadena, CA, 1997), and references therein.
[17] P. O. Wennberg, J. G. Anderson, and D. K. Weisenstein, J. Geophys. Res. **99**, 18839 (1994), and references therein.
[18] M. A. A. Clyne and I. S. McDermid, J. Chem. Soc., Faraday Trans. **71**, 2189 (1975).
[19] J. V. Michael and K. P. Lim, J. Chem. Phys. **97**, 3228 (1992).
[20] D. E. Siskind and D. W. Rusch, J. Geophys. Res. **97**, 3209 (1992).
[21] J. L. Fox, J. Geophys. Res. **99**, 6273 (1994).
[22] T. Kurotaki, AIAA paper No. 2000-2366, 2000.
[23] P. Defazio, C. Petrongolo, P. Gamallo, and M. González, J. Chem. Phys. **122**, 214303 (2005).
[24] G. Black, R. L. Sharpless, and T. G. Slanger, J. Chem. Phys. **58**, 4792 (1973).